Supporting information

Cryogenic Luminescent Tb/Eu-MOF Thermometer Based on a Fluorine-Modified Tetracarboxylate Ligand

Dian Zhao[*,†,‡], Dan Yue[‡], Ling Zhang[‡], Ke Jiang[‡] , and Guodong Qian[*,‡]

[†]Key Laboratory of the Ministry of Education for Advanced Catalysis Materials, Department of Chemistry, Zhejiang Normal University, Jinhua, 321004, China.

[‡]State Key Laboratory of Silicon Materials, Cyrus Tang Center for Sensor Materials and Applications, School of Materials Science and Engineering, Zhejiang University, Hangzhou 310027, China.

*Corresponding Author:

dzhao@zjnu.edu.cn; gdqian@zju.edu.cn;

Table S1. Crystallographic Data collection and Refinement result for **TbFTPTC**.

	TbFTPTC
chemical formula	$C_{144}H_{72}F_5N_4O_{64}Tb_8$
formula weight	4248.41
temperature (K)	293(2)
wavelength (Å)	0.71073
crystal system	Monoclinic
space group	*C* 2/*m*
a (Å)	18.814(4)
b (Å)	27.119(5)
c (Å)	18.985(4)
α (º)	90.00
β (º)	92.25(3)
γ (º)	90.00
V (Å^3)	9679(3)
Z	2
density (calculated g/cm^3)	1.458
absorbance coefficient (mm^{-1})	2.961
F(000)	4082
R (int)	0.1088
goodness of fit on F^2	0.875
R1, wR2 [I>2σ(I)][a]	0.0458, 0.0952
R1, wR2 (all data)[a]	0.0806, 0.1049

R1 = $\Sigma(|F_o| - |F_c|) / \Sigma|F_o|$; wR2 = $[\Sigma w(|F_o|-|F_c|^2) / \Sigma w F_o^2]^{1/2}$.

Table S2. The molar ratio of the starting Eu/Tb salt and that in Eu_xTb_{1-x}FTPTC product calculated by ICP analysis.

Sample	The molar ratio of the starting Tb/Eu salt	The molar ratio of Tb/Eu salt calculated by ICP analysis
$Tb_{0.95}Eu_{0.05}$FTPTC	0.95:0.05	0.9524:0.0476
$Tb_{0.90}Eu_{0.10}$FTPTC	0.90:0.10	0.8913:0.1087
$Tb_{0.80}Eu_{0.20}$FTPTC	0.80:0.20	0.8385:0.1615

Table S3. Quantum yields of **LnFTPTC** at room temperature.

Sample	Quantum yield Φ(%)
TbFTPTC	14.11
EuFTPTC	20.40
$Tb_{0.95}Eu_{0.05}$FTPTC	17.15
$Tb_{0.90}Eu_{0.10}$FTPTC	18.31
$Tb_{0.80}Eu_{0.20}$FTPTC	19.81

Table S4. Comparing the performance of the LnMOF thermometers in terms of temperature range, maximum relative sensitivity (S_m) and corresponding temperature (T_m).

MOF	Range (K)	S_m ($\%K^{-1}$)	T_m (K)	Ref
$Tb_{0.9931}Eu_{0.0069}$DMBDC	50~200	1.15	200	1
$Tb_{0.9954}Eu_{0.0046}$DMBDC	50~200	0.61	200	
$Tb_{0.9989}Eu_{0.0011}$DMBDC	50~200	0.52	200	
$Tb_{0.50}Eu_{0.50}$PIA	75~275	2.02	275	2
$Eu_{0.09}Gd_{0.98}$DSB	65~300	7.14	65	3
$Tb_{0.957}Eu_{0.043}$cpda	40~300	16	300	4
$Tb_{0.8}Eu_{0.2}$L	40~300	0.15	300	5
$[(Tb_{0.9382}Eu_{0.0616})(bpcd)_2(NO_3)_2]\cdot Cl$	25~200	0.34	200	6
$Tb_{0.95}Eu_{0.05}$HL	4~300	31	4	7
$Eu_{0.0878}Tb_{0.9122}$(TPI)	75~250	4.92	250	8
$Tb_{0.95}Eu_{0.05}$BTB	10~320	2.85	14	9
$[(Tb_{0.914}Eu_{0.086})_2(PDA)_3(H_2O)]\cdot 2H_2O$	10~325	5.96	25	10
$(Me_2NH_2)_3[Eu_3(FDC)_4(NO_3)_4]\cdot 4H_2O$	12~320	2.7	170	11

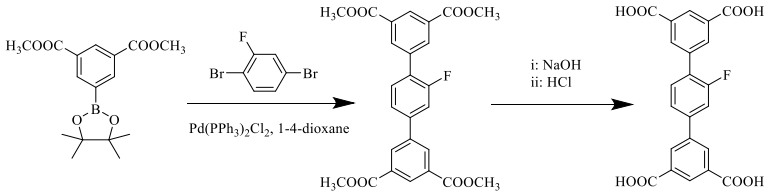

Scheme S1. Synthesis of the organic ligand H_4FTPTC applied to construct **LnFTPTC**.

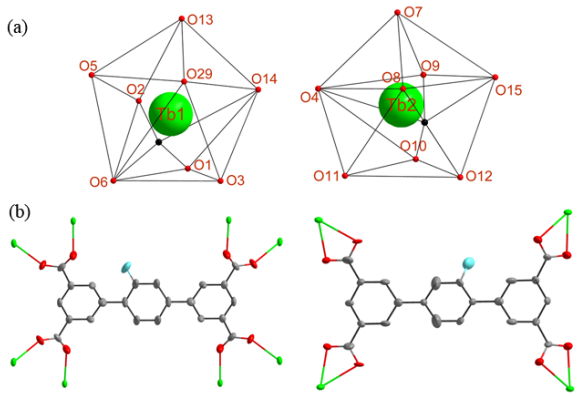

Figure S1. (a) Coordination polyhedron of Tb^{3+} ions; (b) the coordination environments of ligand H_4FTPTC with 30% thermal ellipsoids. Tb^{3+}, green; O, red; C, grey; H atoms are omitted for clarity.

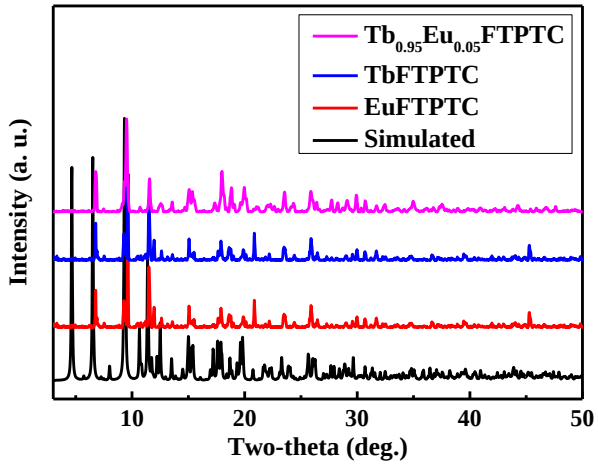

Figure S2. Powder XRD patterns of **EuFTPTC**, **TbFTPTC** and **$Eu_{0.95}Tb_{0.05}$FTPTC**.

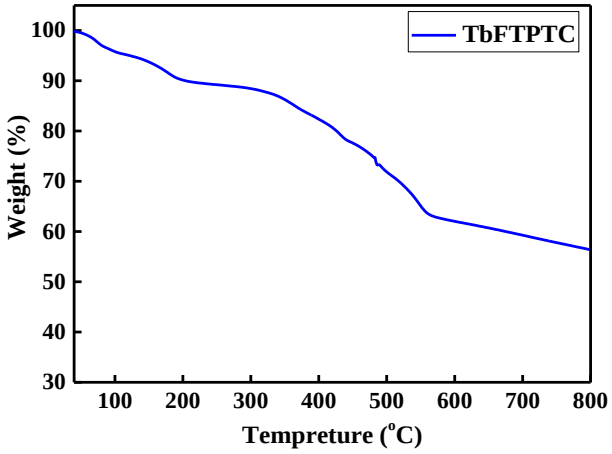

Figure S3. TG curves of **TbFTPTC**.

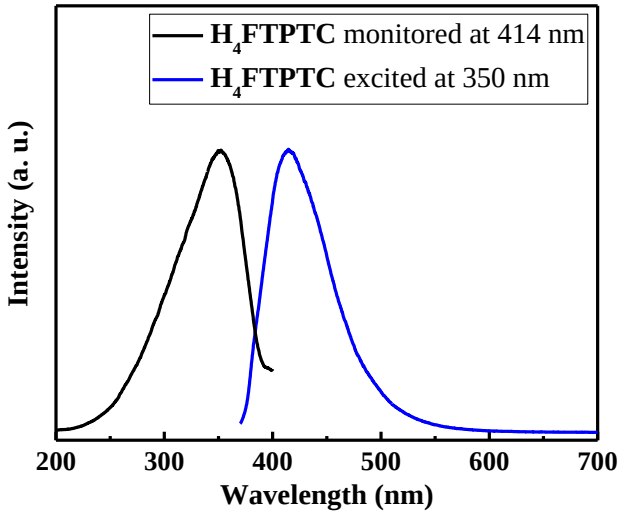

Figure S4. Excitation and emission spectra of the ligand H_4FTPTC.

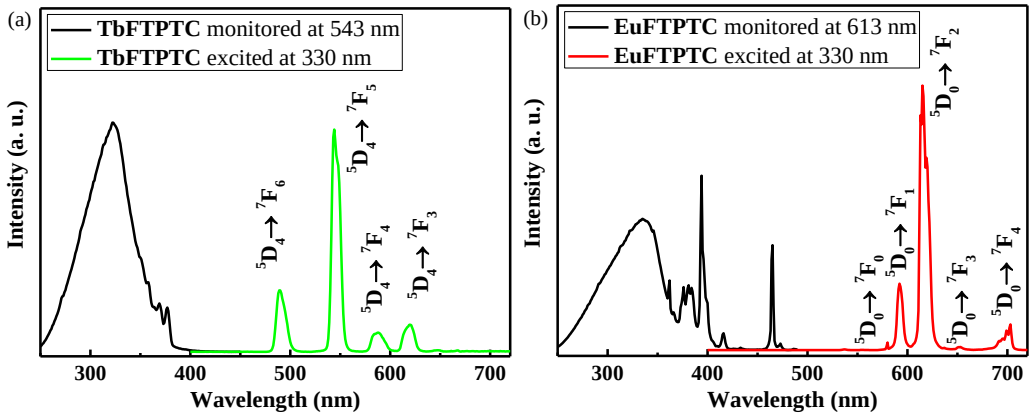

Figure S5. Excitation and emission spectra of (a) **TbFTPTC** and (b) **EuFTPTC**.

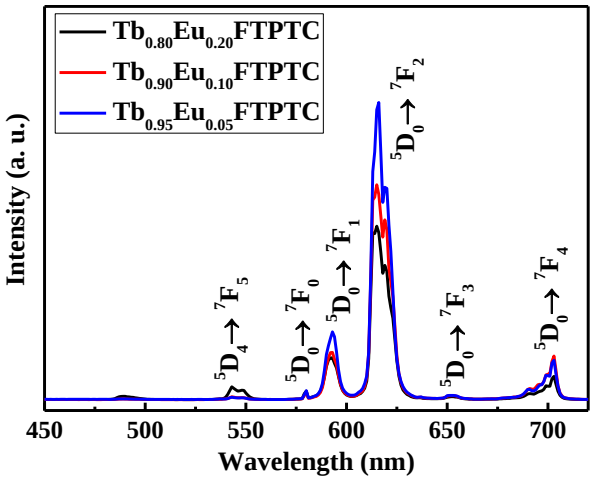

Figure S6. Emission spectra of $Tb_{1-x}Eu_x$FTPTC.

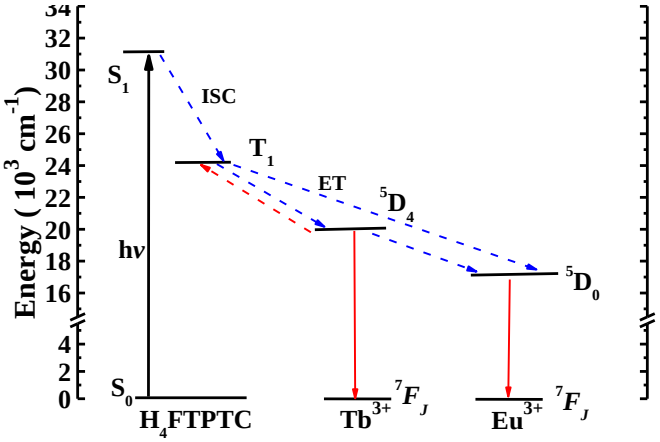

Figure S7. Schematic representation of the energy transfer from the H_4FTPTC to Tb^{3+} ($^5D_4$) and Eu^{3+} ($^5D_0$) ions. (hν = energy absorption; S = singlet; T = triplet; ISC = intersystem crossing; ET = energy transfer).

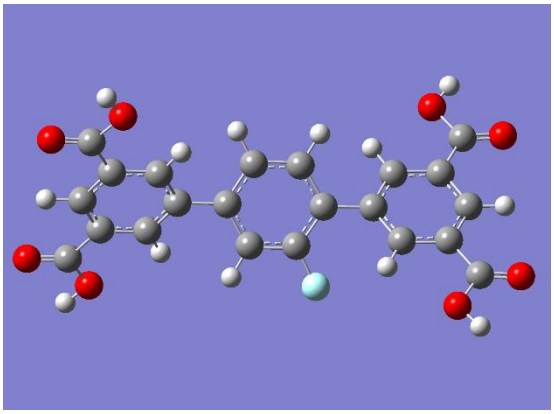

Figure S8. The optimized geometry of free ligands H_4FTPTC. The molecular geometry optimization and frequency analysis of H_4FTPTC were performed using density functional theory (DFT) at the B3LYP/6-31+G(d,p) level,[12] and the optimized geometry was shown in Figure S8. Based on the optimized result, the energy of the lowest triplet excited state (T_1) of the H_4FTPTC were calculated to be 2.9801 eV (24037 cm^{-1}) by the time-dependent DFT approach.[13] All calculations were performed using Gaussian 09 software.[14] It is necessary to note that modification of organic ligands with fluorine atom can affect the T_1 energy of the ligand. In our work, we have demonstrated that modification of [1,1':4',1"-terphenyl]-3,3",5,5"-tetracarboxylic acid with one atom can get a ligand H_4FTPTC with suitable T_1 energy for luminescent Tb/Eu-MOF applied in cryogenic temperature range. Since the strong electron-withdrawing properties, it can be inferred that adding more fluorine atoms on the benzene ring of the [1,1':4',1"-terphenyl]-3,3",5,5"-tetracarboxylic acid would increase the T_1 energy to a too-high level, which is not suitable for our mission.

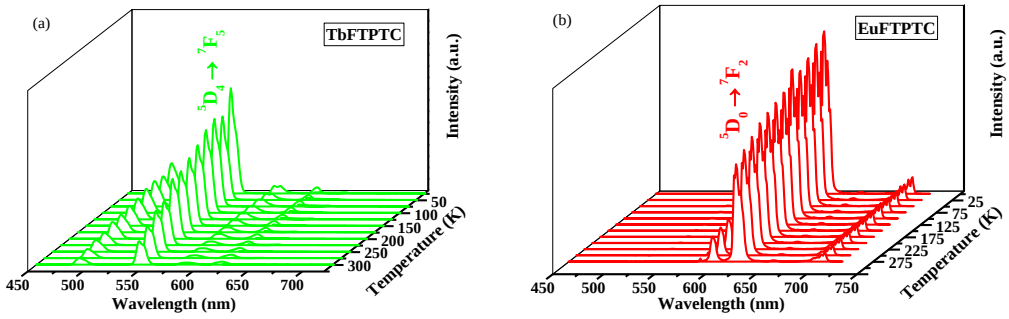

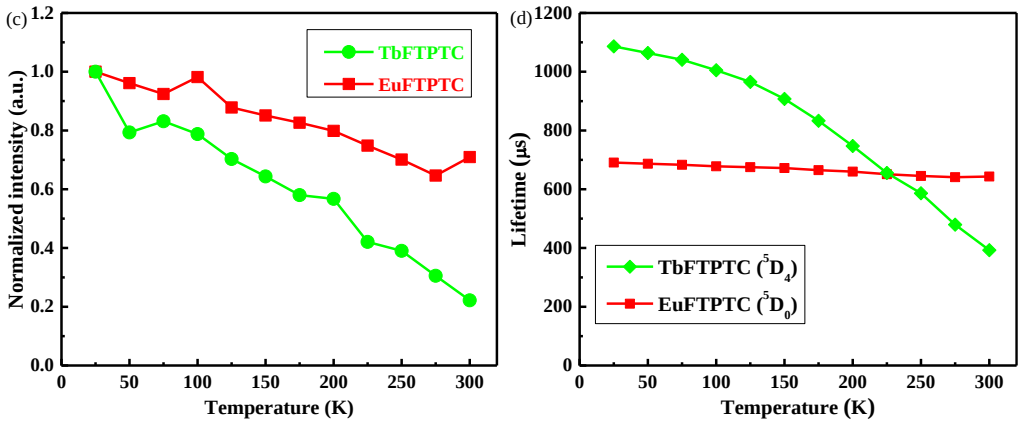

Figure S9. Emission spectra of (a) **TbFTPTC** and (b) **EuFTPTC** recorded between 25 and 300 K; (c) temperature dependent normalized intensity ratio of Tb ($^5D_4 \rightarrow {}^7F_5$) and Eu ($^5D_0 \rightarrow {}^7F_2$) for **TbFTPTC** and **EuFTPTC**, respectively ; (d) Temperature dependence of the $^5D_4$ lifetime for **TbFTPTC** and $^5D_0$ lifetime for **EuFTPTC**, respectively. (excited at 330 nm).

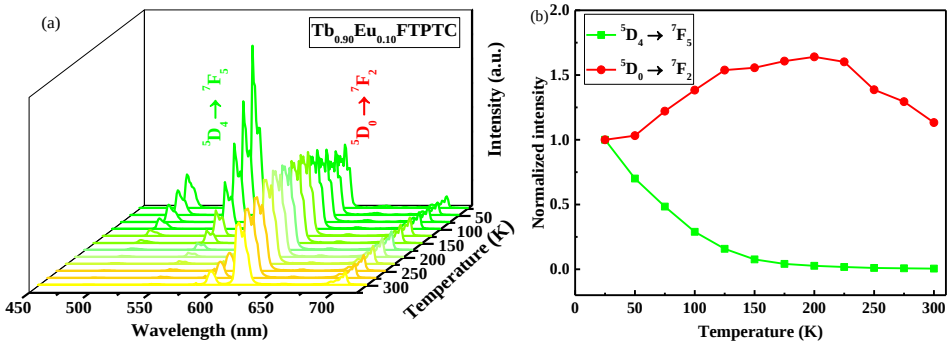

Figure S10. Emission spectra of (a) **$Tb_{0.90}Eu_{0.10}$FTPTC** recorded between 25 and 300 K; (b) temperature dependent normalized intensity ratio of Tb^{3+} ($^5D_4 \rightarrow {}^7F_5$) and Eu^{3+} ($^5D_0 \rightarrow {}^7F_2$) for **$Tb_{0.90}Eu_{0.10}$FTPTC**.

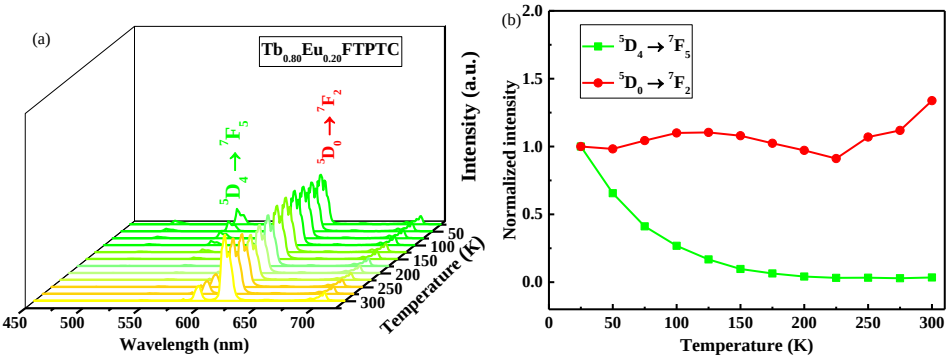

Figure S11. Emission spectra of (a) **$Tb_{0.80}Eu_{0.20}$FTPTC** recorded between 25 and 300 K; (b) temperature dependent normalized intensity ratio of Tb ($^5D_4 \rightarrow {}^7F_5$) and Eu ($^5D_0 \rightarrow {}^7F_2$) for **$Tb_{0.80}Eu_{0.20}$FTPTC**.

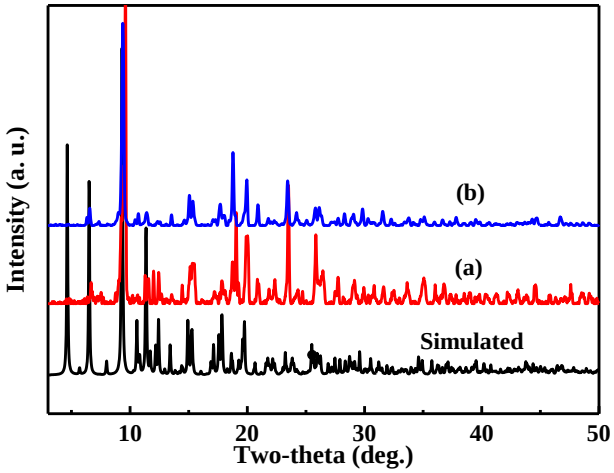

Figure S12. Powder XRD patterns of **$Eu_{0.95}Tb_{0.05}$FTPTC** (a) after cryogenic photoluminescence measurements and (b) under room conditions for three months.

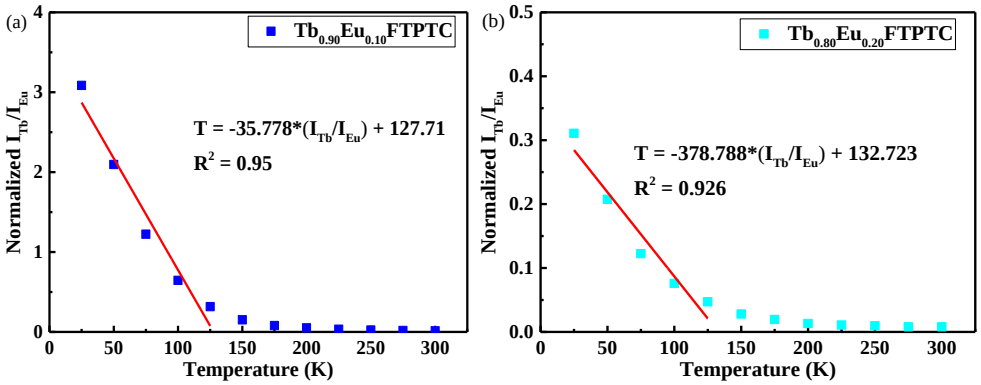

Figure S13. Temperature-dependent intensity ratio of Tb^{3+} (543 nm) and Eu^{3+} (613 nm) and the fitted curve for (a) **$Tb_{0.90}Eu_{0.10}$FTPTC** and (b) **$Tb_{0.80}Eu_{0.20}$FTPTC**.

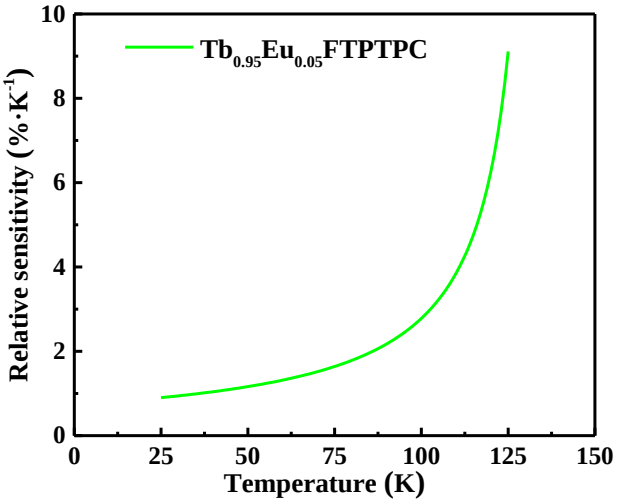

Figure S14. Temperature-dependent generalized relative sensitivity of **$Tb_{0.95}Eu_{0.05}$FTPTC**.

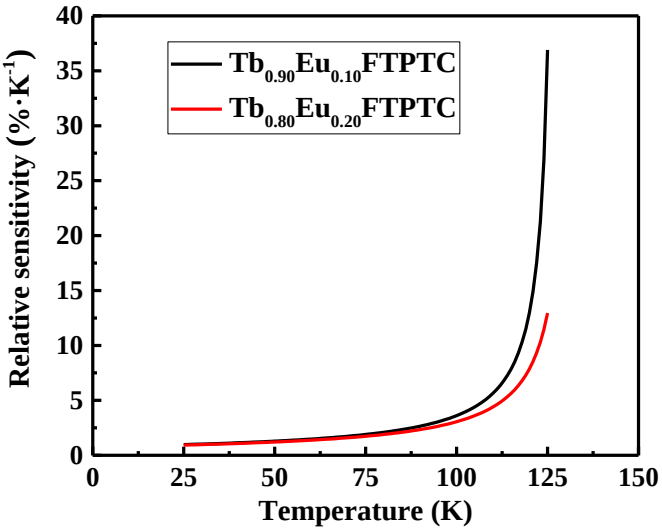

Figure S15. Temperature dependence of the relative sensitivity for **$Tb_{0.90}Eu_{0.10}$FTPTC** and **$Tb_{0.80}Eu_{0.20}$FTPTC** in the range of 25 to 125 K.

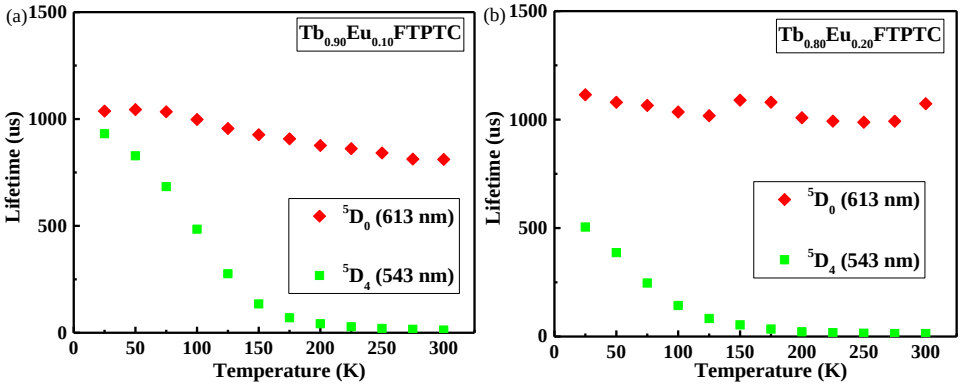

Figure S16. Temperature dependence of the $^5D_4$ (Tb^{3+}, 543 nm) and $^5D_0$ (Eu^{3+}, 613 nm) lifetime for (a) **$Tb_{0.90}Eu_{0.10}$FTPTC** and (b) **$Tb_{0.90}Eu_{0.20}$FTPTC**.

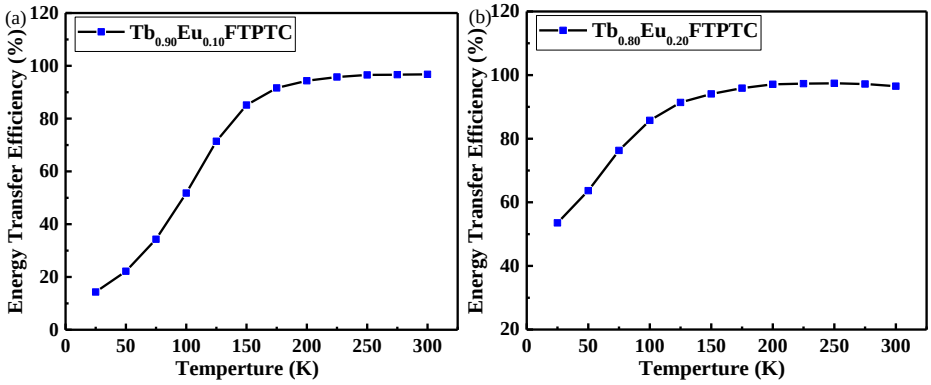

Figure S17. Temperature dependence of energy transfer efficiency from Tb^{3+} to Eu^{3+} of (a) **$Tb_{0.90}Eu_{0.10}$FTPTC** and (b) **$Tb_{0.80}Eu_{0.20}$FTPTC**.

Reference

(1) Cui, Y.; Xu, H.; Yue, Y.; Guo, Z.; Yu, J.; Chen, Z.; Gao, J.; Yang, Y.; Qian, G.; Chen, B. A luminescent mixed-lanthanide metal-organic framework thermometer. *J. Am. Chem. Soc.* **2012**, *134*, 3979-3982.

(2) Rao, X.; Song, T.; Gao, J.; Cui, Y.; Yang, Y.; Wu, C.; Chen, B.; Qian, G. A highly sensitive mixed lanthanide metal-organic framework self-calibrated luminescent thermometer. *J. Am. Chem. Soc.* **2013**, *135*, 15559-15564.

(3) D'Vries, R. F; Álvarez-García, S.; Snejko, N.; Bausá, L. E.; Gutiérrez-Puebla, E.; de Andrés, A.; Monge, M. Á. Multimetal rare earth MOFs for lighting and thermometry: tailoring color and optimal temperature range through enhanced disulfobenzoic triplet phosphorescence. *J. Mater. Chem. C* **2013**, *1*, 6316-6324.

(4) Cui, Y.; Zou, W.; Song, R.; Yu, J.; Zhang, W.; Yang, Y.; Qian, G. A ratiometric and colorimetric luminescent thermometer over a wide temperature range based on a lanthanide coordination polymer. Chem. Commun. **2014**, 50, 719-721.

(5) Zhao, S.-N.; Li, L.-J.; Song, X.-Z.; Zhu, M.; Hao, Z.-M.; Meng, X.; Wu, L.-L.; Feng, J.; Song, S.-Y.; Wang, C.; Zhang, H.-J. Lanthanide Ion Codoped Emitters for Tailoring Emission Trajectory and Temperature Sensing. *Adv. Funct. Mater.* **2015**, *25*, 1463-1469.

(6) Meng, X.; Song, S.-Y.; Song, X.-Z.; Zhu, M.; Zhao, S.-N.; Wu, L.-L.; Zhang, H.-J. A Eu/Tb-codoped coordination polymer luminescent thermometer. *Inorg. Chem. Front.* **2014**, *1*, 757-760.

(7) Liu, X.; Akerboom, S.; Jong, M. D.; Mutikainen, I.; Tanase, S.; Meijerink, A; Bouwman, E. Mixed-lanthanoid metal–organic framework for ratiometric cryogenic temperature sensing. *Inorg. Chem.* **2015**, *54*, 11323-11329.

(8) Wu, L.-L.; Zhao, J.; Wang, H.; Wang, J. A lanthanide(III) metal–organic framework exhibiting ratiometric luminescent temperature sensing and tunable white light emission. *CrystEngComm* **2016**, *18*, 4268-4271.

(9) Ananias, D.; Brites, C. D. S.; Carlos, L. D.; Rocha. J. Cryogenic nanothermometer based on the MIL-103(Tb,Eu) metal–organic framework. *Eur. J. Inorg. Chem.*, 2016, 2016, 1967-1971.

(10) Wang, Z.; Ananias, D.; Carné-Sánchez, A.; Brites, C. D. S.; Imaz, I.; Maspoch, D.; Rocha, J.; Carlos, L. D. Lanthanide–organic framework nanothermometers prepared by spray-drying. *Adv. Funct. Mater.* **2015**, *25*, 2824-2830.

(11) Li, L.; Zhu, Y.; Zhou, X.; Brites, C. D. S.; Ananias, D.; Lin, Z.; Paz, F. A. A.; Rocha, J.; Huang, W.; Carlos, L. D. Visible-light excited luminescent thermometer based on single lanthanide organic frameworks. *Adv. Funct. Mater.* **2016**, *26*, 8677-8684.

(12) Becke, A. D. Density-functional thermochemistry. III. The role of exact exchange. *J. Chem. Phys.* **1993**, *98*, 5648−5652.

(13) Runge, E.; Gross, E. K. U. Density-functional theory for time-dependent systems. *Phys. Rev. Lett.* **1984**, *52*, 997−1000.

(14) Frisch, M. J.; Trucks, G. W.; Schlegel, H. B.; Scuseria, G. E.; Robb, M. A.; Cheeseman, J. R.; Scalmani, G.; Barone, V.; Mennucci, B.; Petersson, G. A.; Nakatsuji, H.; Caricato, M.; Li, X.; Hratchian, H. P.; Izmaylov, A. F.; Bloino, J.; Zheng, G.; Sonnenberg, J. L.; Hada, M.; Ehara, M.; Toyota, K.; Fukuda, R.; Hasegawa, J.; Ishida, M.; Nakajima, T.; Honda, Y.; Kitao, O.; Nakai, H.; Vreven, T.; Montgomery, J. A., Jr.; Peralta, J. E.; Ogliaro, F.; Bearpark, M.; Heyd, J. J.; Brothers, E.; Kudin, K. N.; Staroverov, V. N.; Keith, T.; Kobayashi, R.; Normand, J.; Raghavachari, K.;

Rendell, A.; Burant, J. C.; Iyengar, S. S.; Tomasi, J.; Cossi, M.; Rega, N.; Millam, J. M.; Klene, M.; Knox, J. E.; Cross, J. B.; Bakken, V.; Adamo, C.; Jaramillo, J.; Gomperts, R.; Stratmann, R. E.; Yazyev, O.; Austin, A. J.; Cammi, R.; Pomelli, C.; Ochterski, J. W.; Martin, R. L.; Morokuma, K.; Zakrzewski, V. G.; Voth, G. A.; Salvador, P.; Dannenberg, J. J.; Dapprich, S.; Daniels, A. D.; Farkas, Ö .; Foresman, J. B.; Ortiz, J. V.; Cioslowski, J.; Fox, D. J. *Gaussian 09*, revision D.01; Gaussian Inc.: Pittsburgh, PA, 2009.